



Original article

Numerical method for the characterization of sea states using realistic irregular waves on computational fluid dynamics simulations for application on wave energy converters

Phelype Haron Oleinik^a, Rafael Pereira Maciel^a, Elizaldo Domingues dos Santos^a, Luiz Alberto Oliveira Rocha^a, Bianca Neves Machado^b, Liércio André Isoldi^{a,*}

^a Programa de Pós-Graduação em Engenharia Oceânica, Escola de Engenharia, Universidade Federal do Rio Grande, Av. Itália s/n, km 8, Campus Carreiros, Rio Grande, 96201-900, RS, Brazil

^b Programa de Pós-Graduação em Matemática Aplicada, Universidade Federal do Rio Grande do Sul, Av. Bento Gonçalves, 9500, Campus do Vale, Porto Alegre, 91509-900, RS, Brazil

ARTICLE INFO

Keywords:

Renewable energy
Realistic irregular waves
WaveMIMO methodology
Fluent
Wave energy converter

ABSTRACT

Energy demand grows along with technological advances, industrial expansion, and global urbanization. To supply this demand sustainably, there are several attempts to harness energy from renewable sources, among them, wave energy. The study of wave energy availability in energy conversion devices primarily focuses on two major areas: analysis of the fluid-dynamic behavior of the devices and the simulation of sea states to estimate theoretical energy potential. Despite advancements in both fields, there is a lack of methodologies that effectively integrate realistic irregular wave simulations and fluid-dynamic analysis of energy conversion devices. This research aims to integrate these areas by employing the WaveMIMO methodology, in which a sea state spectrum is converted into a statistically equivalent time series of water free surface elevation, then applied as an estimation of the velocity field in the water column to generate irregular waves. This study focuses on the development of a methodology to characterize the wave climate in the city of Rio Grande, in southern Brazil, for the year 2014, using a histogram to classify sea states according to their significant wave height and mean wave period, thus producing a bivariate histogram of wave conditions. A sea state spectrum was obtained for each pair of wave height and period and simulated using the computational fluid dynamics software Fluent to reproduce the realistic irregular waves of this sea state. The results indicated that the methodology for categorizing the sea state based on a histogram proved to be a computationally efficient alternative for the numerical simulation of wave climates in a given location for a long period of time, reducing the simulation time needed to approximately 0.5% of the total amount. In addition, an application of this methodology to investigate the wave energy conversion employing an oscillating water column device is presented as supplementary material.

Introduction

Renewable energies have emerged as a solution to the challenges of climate change and the depletion of non-renewable resources. According to the International Energy Agency (IEA), renewable sources accounted for around 29% of global electricity generation in 2020, showing a significant increase compared to previous years. The IEA forecasts that this share will rise to 37% by 2026, driven by continued investments and supportive policies [1]

Ocean wave energy is a promising renewable power source, offering high availability and relatively untapped potential. While the precise estimation of theoretically available wave power is not definitive [2–5],

approximate figures hover around 27 000 TWh/year, exceeding the renewable energy generation target of 12 000 TWh set by the IEA for the year 2026. Several countries have initiated projects and trials to explore the potential of wave energy, most notably Portugal [6], the United Kingdom [7], and Australia [8], but none of the deployed prototypes have reached commercial scale, partly due to the different technologies which compete for research and development focus, and partly due to the various location sites that have contrasting characteristics, making development even more complex [5].

Given the challenges in making wave energy harvesting a feasible reality, this paper presents a numerical methodology for a simple and

* Corresponding author.

E-mail address: liercioisoldi@furg.br (L.A. Isoldi).

<https://doi.org/10.1016/j.seta.2024.104093>

Received 22 July 2024; Received in revised form 10 November 2024; Accepted 14 November 2024

Available online 29 November 2024

2213-1388/© 2024 Elsevier Ltd. All rights reserved, including those for text and data mining, AI training, and similar technologies.

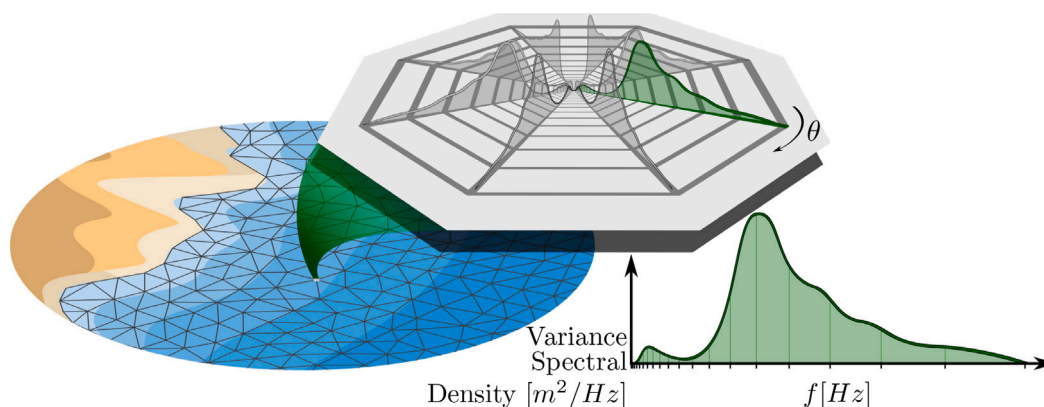


Fig. 1. Illustration of a finite element mesh and directional wave spectrum for a given propagation direction.

cost-effective initial investigation of the expected energy output of a wave energy converter (WEC) at any location. This methodology is applicable regardless of the WEC type or geographical location, enabling rapid estimation of the expected energy output. This allows researchers and investors to make more informed decisions about the most suitable device and location for installation.

In this context, spectral wave models are useful for long-term simulations of the wave climates, and their results can be used to assess long-term trends and variability in the wave climate [4,9–12] and the theoretical wave power delivered by the waves [2,3,13].

However, spectral wave models cannot properly simulate WECs. Firstly, because they operate in the frequency domain, while computational fluid dynamics (CFD) models of the devices operate in the time domain, therefore, they are incompatible in their very nature. Secondly, because of the time scales involved: spectral models usually simulate periods of one year or longer, using time steps of about 15 min, while CFD models usually simulate periods of only a few minutes, using time steps typically shorter than 1 s.

That said, this paper aims to combine these two approaches to estimate the available power that can be extracted from a WEC. To that end, the WaveMIMO methodology [14] uses spectral wave data for the characterization of the wave climate in the study area and as a data source for boundary conditions. Then, it transforms the wave spectrum from the frequency to the time domain, using it as boundary conditions for the CFD model.

The entirety of the WaveMIMO methodology as applied in the present research consists in 6 steps:

1. Spectral simulation of the waves in the study area, in this paper, using the third-generation wave model TOMAWAC;
2. Analysis of the results of the spectral model for the characterization of the wave climate and definition of the simulation plan;
3. Transformation of the selected wave spectra into time series of sea surface elevation;
4. Computation of the boundary conditions for the CFD model;
5. CFD simulation of the selected cases;
6. Analysis of the results and estimation of the wave power deliverable by the simulated WEC device if installed in the chosen location.

It is worth mentioning that steps 3 and 4 are thoroughly explained by Oleinik et al. [15] and Machado et al. [14], respectively, so an abridged version was presented in this study, for brevity.

Materials and methods

The application of the WaveMIMO methodology involved two parts. First (frequency domain), the study area was defined, and a spectral

wave model was selected, run, and converted to the time domain for a chosen spatial point. Second (time domain), the CFD model was selected, and the time-domain data was adjusted for suitable boundary conditions, allowing the CFD model to simulate realistic irregular wave generation and propagation.

Sea state simulation and study area

The adopted spectral wave model was TOMAWAC [16,17], a third-generation spectral wave model that solves the wave action conservation equation on a discrete domain employing the finite element method. To do so, TOMAWAC discretizes the waves on each node of the domain in a finite number of wave frequencies and propagation directions, called directional wave spectrum, illustrated in Fig. 1.

For this paper, the study area chosen for the WEC device was the coast of the municipality of Rio Grande, in the state of Rio Grande do Sul, Brazil. The simulation domain encompassed the entire geographical state, as shown in Fig. 2, along with the numerical mesh used for the sea state simulation. The coastline shape was taken from the GSHHG¹ (Global Self-consistent, Hierarchical, High-resolution Geography Database) [18].

The spatial discretization varied, with element edges ranging from 10 km at the offshore mesh border to 1.3 km at the continental shelf break and 250 m along the coastline. A 15-min time step was used for temporal discretization, with 25 wave frequencies per direction in the spectral discretization. This setup was used in prior studies on the southern Brazilian coast [12–14,19,20].

At the oceanic boundaries (red shading contour in Fig. 2), spectral parameters taken from NOAA (National Oceanic and Atmospheric Administration)'s WAVEWATCH III historical data² were obtained and interpolated to the boundary nodes of the mesh. The parameters, namely, significant wave height (H_s), spectral peak period (T_p), and principal peak direction (D_p), were used as parameters to compute a JONSWAP (Joint North Sea Wave Observation Project) wave spectrum [21] at each mesh node, which was then used as the boundary condition for TOMAWAC. On the water surface, wind from NOAA's *Reanalysis 1* project³ was used as boundary condition.

Finally, data from the GEBCO⁴ (General Bathymetric Chart of the Oceans) were used to represent the bottom bathymetry in the deep ocean, and on the continental shelf, nautical charts from the Brazilian Navy⁵ were obtained and digitalized into a bathymetry database [22], which was used to form the bathymetry for this study.

¹ www.ngdc.noaa.gov/mgg/shorelines/gshhs.html

² ftp://polar.ncep.noaa.gov/history/waves/multi_1

³ www.esrl.noaa.gov/psd/data/gridded/data.ncep.reanalysis.html

⁴ www.gebco.net

⁵ <https://www.marinha.mil.br/chm/dados-do-segnav-cartas-nauticas>

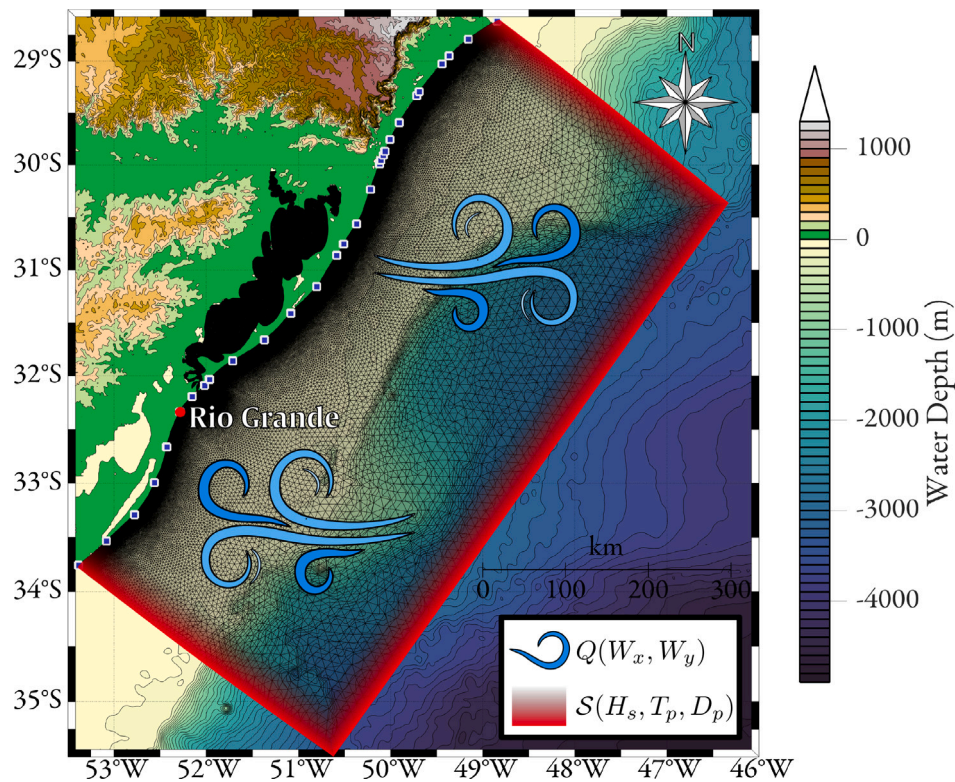


Fig. 2. Overview of the study area and the numerical mesh used.

The simulation was then run for the entire year of 2014, and the complete directional wave spectrum was collected at the selected node (Rio Grande), and saved at each time step of 15 min.

Definition of the simulation plan

An advantage of CFD is its ability to quantify the energy a WEC would capture if installed at a chosen location. However, due to the high variability of ocean waves, simulating a long period is required for accurate estimates. Simulating a full year of sea states with CFD is infeasible, so simplifications were necessary. This involved statistical analysis of the wave climate using TOMAWAC results to generate a time series of H_s and T_m (mean wave period), classified in a bivariate histogram (Fig. 3) showing the occurrence frequency of each H_s and T_m combination. The histogram's bin count was estimated using the Freedman–Diaconis rule [23].

Each data point accounted for in the histogram represents a wave spectrum of a 15 min time step, from a total of 35 040 occurrences. The most frequent scenario has H_s of 0.66 ± 0.06 m and T_m of 6.3 ± 0.3 s, which accounts for 5.88% of the dataset.

Considering that H_s and T_m are suitable parameters to describe a sea state, it is admissible that the histogram in Fig. 3 adequately describes the sea state in the studied location and time interval, as it shows, approximately, how often each sea state occurs. This is not completely accurate, as the sea state cannot be perfectly described by just H_s and T_m , instead of a complete spectrum. However, using these average parameters is a good first approximation of the spectrum, even more so in shallower areas, where bottom friction dissipates longer waves, making the wave spectra more uniform.

Therefore, by using the histogram to characterize the sea state, the number of simulated cases could be reduced from 35 040 (one every 15 min for a year) to 181 (pairs of H_s and T_m with at least one occurrence in Fig. 3).

To select the simulated cases, all spectra that contributed to each bin in the histogram were averaged at each wave frequency. Then, each

spectrum was compared to the average spectrum using the least squares difference metric to find the one closest to the average. That spectrum was selected to represent the entire bin in the histogram. This process was repeated for all 181 bins.

CFD model

For the simulations, CFD software Fluent 19.3 (2019 R2 academic) was used. Fluent, a finite volume-based general-purpose CFD code [24, 25], simulated a wave flume following previous studies [14,26–28]. The study assumed laminar, incompressible flow to model wave propagation and interaction with air, the device, and the wave flume. To this end, Fluent solves the mass and momentum conservation equations [24].

To simulate the wave flume, a fraction of the domain must be filled with water and the remaining volume with air. To treat the two-phase flow in the flume, this study employed the volume of fluid method [29,30], allowing to simulate the interface between fluids in a multiphase immiscible flow. Additionally, Fluent also solves an equation of transport of the quantity called volume fraction for each phase in the flow [30].

Furthermore, a numerical beach condition was applied at the end of the wave channel to dissipate waves, mimicking natural beach wave dissipation. This prevented reflections that could disturb the channel inlet and interfere with the imposed sea state. The condition added an energy source term to the momentum equation, with damping coefficients of 20 s^{-1} for linear and 0 m^{-1} for quadratic, as recommended in [27].

Prescribed velocity data for the CFD simulation

Each simulated spectrum had to be converted into proper time-domain boundary condition data for the CFD simulation. As the numerical model used in this study uses prescribed velocity boundary conditions, each wave spectrum must be transformed into a time-varying vertical profile of the water velocity caused by the waves.

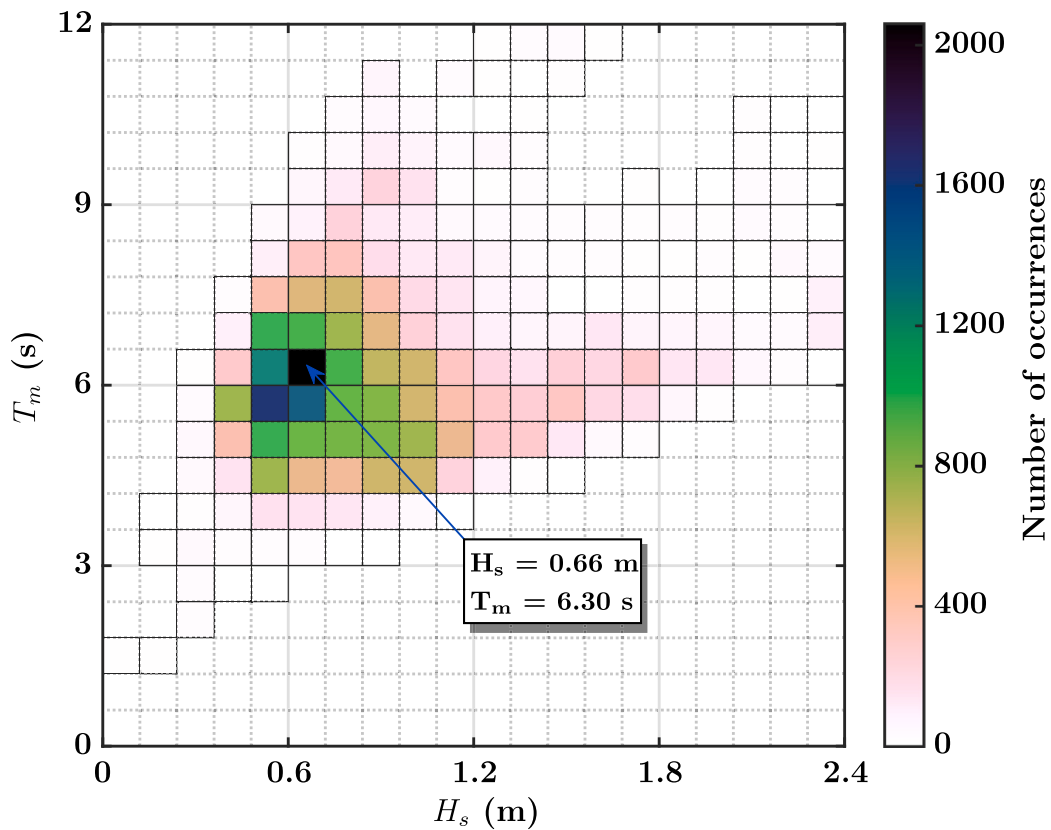


Fig. 3. Bivariate histogram of H_s and T_m on the study location.

To that end, firstly, the spectrum was transformed into a time series of water surface elevation (η) using the method proposed by Oleinik et al. [15], which uses the wave amplitude spectrum and a random phase spectrum to generate a valid Fourier transform of a time series of η , which then went through an Inverse Fourier transform to produce the time series of η .

The converted time series was then used to count and measure the period of each wave using the zero-up crossing method. The discrete period measured was then cosine-interpolated into a time series, T , with the same length as the time series of η . With that and the local water depth, d , it was possible to solve the dispersion relation for the wavelength, L . This method is entirely linear and could be replaced by the method by Rienecker and Fenton [31], or the one by Chang and Lin [32]. However, as shown by Machado et al. [14], the velocity profiles generated using this fully linear method match the initial time series of η quite closely, so, in practice, the added complexity is only effective if a much higher degree of accuracy is required.

With the time series of water surface elevation, wave period, and wavelength, it was possible to compute the time series of water velocity in the x and z directions [33,34].

The numerical model

To simulate the WEC under wave action, it must be placed in a wave flume to capture wave-device interactions. The flume design followed Martins et al. [35], with a total length of 327 m, a water depth of 10 m (based on the study location, red dot in Fig. 2), and an additional 5 m above the surface to avoid top boundary interactions. Fig. 4 shows a schematic of the wave flume.

At the bottom of the wave flume (continuous black line), a non-slip boundary condition was imposed to simulate the bottom friction, and at the top and on the left boundary above the free surface (dashed red line), a boundary condition of constant atmospheric pressure was prescribed to allow free air flow.

The velocity inlet boundary condition to the left (continuous blue line) was the only boundary where waves were prescribed into the model. In this boundary, the velocity data obtained as previously mentioned were used along the water column. In the inlet, below the free surface, the boundary was divided into a specific number of segments, and, for each segment i at an average depth z_i , a time series of u and w was generated, to compose the prescribed velocity vector \bar{u} as shown in Fig. 5. This velocity vector was imposed on every mesh element whose edge overlapped the segment.

The wave flume had two well-defined regions. The first region accounted for two-thirds of the flume, where the waves were generated and propagated, and the WEC device was inserted. The second region consisted of one-third of the flume, with a numerical beach to dissipate incoming waves, represented by the green shaded area in Fig. 4.

Discretization

To ensure that the waves imposed at the boundary were correctly inserted in the model and that they propagate properly to the location of the WEC, the spatial discretization of the computational domain, as well as the temporal discretization of the numerical simulation, must be examined. In addition to that, the ideal amount of inlet segments (z_i in Fig. 5) should be determined.

Therefore, three types of tests were performed: time step (Δt), size of mesh elements (Δs), and size of the inlet segments (Δz). These parameters were tested with each other, using the most extreme sea state (highest H_s) in the database. The results were collected at the flume inlet, and 109 m away from the inlet, where the WEC would be simulated.

Reference values of Δt and Δs were obtained from previous works, then, a larger and a smaller value were tested for each. For Δt , the reference value of 0.05 s [14,36] was used, and the values 0.03 s and 0.07 s were tested. For Δs , the reference value was derived from Martins et al. [35], yielding elements with a nominal edge length of 0.3 m, and

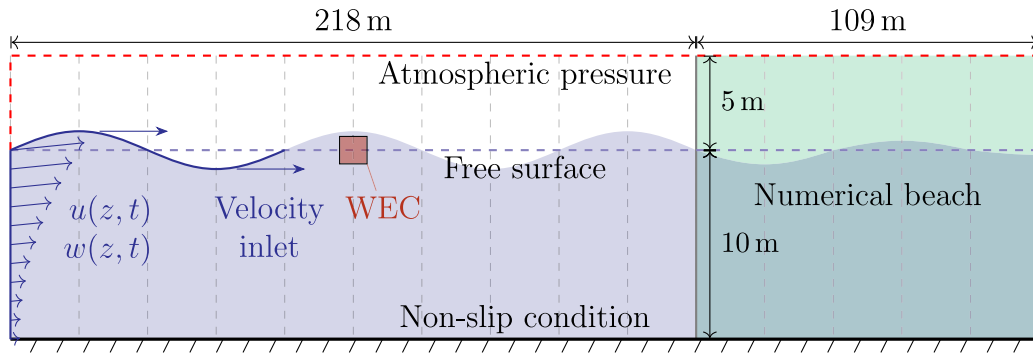


Fig. 4. Schematic illustration of the wave flume (vertical scale exaggerated by a factor of approximately 120).

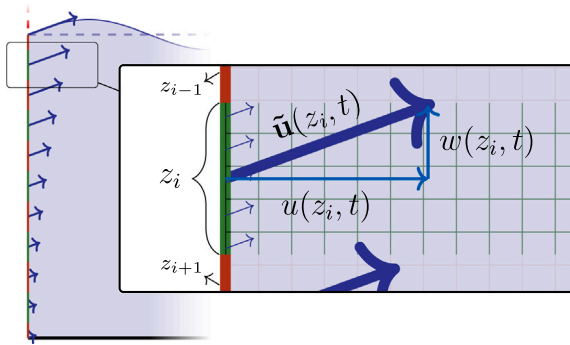


Fig. 5. Schematic illustration of the wave flume inlet, where the prescribed velocity is imposed as a boundary condition.

additionally, 0.2 m and 0.5 m were tested. In turn, the bibliography for the size of the inlet segments [14] suggests 14 divisions along the inlet boundary. Based on that and aiming to ensure a good representation of the prescribed velocities, the inlet boundary was divided into 15, 25, and 50 segments. The three values for each of the three parameters were tested with each other, in turn, resulting in 27 simulations.

The duration of each simulation was 5 min, using the same time series of η as basis for each of them. Simulations were executed on an Intel® Core™ i5-9600K@4.6 GHz with 16 GB RAM @ 2400 MHz, with run times ranging from 74 min to 27 h, depending on discretization. All simulations used four processor cores in parallel.

Since the main variable of interest in this work was η , it was used to assess the performance of each of the tests. To compare the simulations, the root mean square deviation (RMSD) was employed [37].

Results and discussion

Free surface elevation results were compared with input data to verify proper domain discretization and the model's accuracy in reproducing the imposed sea state. This verification ensured that Fluent-simulated waves matched the boundary conditions and maintained their characteristics through the domain, allowing accurate estimation of the WEC's available power and energy.

Discretization

The initial results showed that the different values of Δz presented an irrelevant impact on the results. The RMSD between the simulations with 15 and 25 segments was 0.003 m, and between 25 and 50 was 0.0015 m. In both cases, differences were 3 orders of magnitude less than the values of η , therefore the difference was, in practice, negligible. Possibly, a further reduction of the number of segments

Table 1

RMSD (in m) between the 15 simulations using 25 segments and the reference time series of η .

Δs (m)	Δt (s)				
	0.07	0.05	0.03		
0.8	0.2067	0.2057	0.2043	0.2056	
0.5	0.1802	0.1784	0.1766	0.1784	-13.230%
0.3	0.1717	0.1699	0.1684	0.1700	-4.709%
0.2	0.1629	0.1608	0.1593	0.1610	-5.294%
0.1	0.1584	0.1557	0.1537	0.1559	-3.168%
	0.1760	0.1741	0.1725	RMSD	
		-1.0795%	-0.9190%		Difference

to fewer than 15 could result in a considerable loss of detail in the input boundary conditions. Therefore, for this work, the setup with 25 segments was chosen, which accounted for Δz equal to 0.4 m. One can highlight that the number of segments did not impact the simulation time, since mesh discretization did not change. The only disadvantage of more segments is the larger effort to load the boundary condition data.

Thus, with Δz chosen, 9 simulations were left to be compared. However, with these simulations, the results to determine which discretization was best were inconclusive, therefore, two new values for Δs were analyzed, i.e., 0.1 m and 0.8 m. The results of the RMSD computed for each of the 15 simulations are summarized in Table 1.

The bold values in the additional rows and columns in Table 1 show the average value of RMSD for each column and row, respectively, and next to it, the percentage difference to the previous average. For example, the average of the first two rows is, respectively, 0.2056 m and 0.1784 m, and the relative difference between the two is -13.230%. The highlighted value of RMSD corresponds to the discretization adopted for the rest of this paper.

Table 1 shows that changes in Δt improved the result by an average of 1%, while the changes in Δs improved the results by around 5%. It should be noted that, while the change of Δs from 0.8 m to 0.5 m considerably improved the result, the change in element size is also larger in that case, so a larger difference is expected.

An important aspect regarding the choice of discretization, along with the accuracy of the results, is the computational time; especially in a work with a large number of simulations. Thus, Table 2 shows the computational time for each of the cases. As in Table 1, the bold values in the additional rows and columns in Table 2 show the average value of the computational time in each column and row, respectively, and next to it, the percentage difference to the previous average.

Table 2 shows a considerable performance improvement depending on the size, and consequently the number, of mesh elements. The mesh with $\Delta s = 0.5$ m (20 590 elements) presented a relatively small increase in the RMSD compared to the other mesh sizes, and a 31% shorter

Table 2
Run time (in h:min) of each of the 15 cases with 25 segments.

Δs (m)	Δt (s)				
	0.07	0.05	0.03		
0.8	01:14	01:25	02:13	01:37	
0.5	01:44	01:48	02:50	02:07	+30.93%
0.3	01:50	02:30	04:00	02:47	+31.50%
0.2	03:30	04:35	07:25	05:10	+85.63%
0.1	12:26	17:20	27:20	19:02	+268.39%
	04:09	05:32	08:46	Time	
		+33.33%	+58.43%		Difference

processing time compared to $\Delta s = 0.3$ m. The case with $\Delta s = 0.8$ m also presented a much shorter computational time, but with much worse results. Compared to the mesh size, the time step has little impact on the results, and there is a considerable increase in processing time from $\Delta t = 0.05$ s to $\Delta t = 0.03$ s, so the former was adopted. In summary, after the tests described above, the discretizations adopted were: $\Delta s = 0.5$ m, $\Delta t = 0.05$ s, and $\Delta z = 0.4$ m.

Computational model verification

Since it is not feasible to present a comparison of all 181 simulations, only three are shown for the model verification, representing the different behaviors observed in the results.

It is important to note that directly comparing free surface elevation time series from different locations is ineffective. This is because wave propagation velocity varies with wavelength, and since the series contains multiple sinusoidal components with different lengths, each propagates at a distinct speed, altering the time series shape as it evolves. This phenomenon is illustrated in Fig. 6, which shows a time series of η measured at the wave channel inlet, overlaid with the elevation at the center of the hydropneumatic chamber of an Oscillating Water Column (OWC) WEC, where both time series are offset from each other due to the wave propagation along the channel. All details about the considered OWC can be found in the supplementary material of this paper.

The time series in Fig. 6(a) show the free surface elevation for case 12×05 (row 12 from the bottom and column 5 from the left of Fig. 3), which presented $H_s = 0.54$ m and $T_m = 6.90$ s.

In Fig. 6(a), the RMSD between the elevation time series from TOMAWAC and that at the channel inlet was 0.092 m. This close match shows that transforming elevation into velocity profiles and applying them as boundary conditions effectively reproduces the original surface elevation, indicating that the WaveMIMO methodology accurately replicates the original sea state at the wave channel inlet.

While Fig. 6(a) depicts a typical case of wave climate in the municipality of Rio Grande, Brazil, and how the WaveMIMO methodology adequately represents this wave climate using irregular waves; Figs. 6(b) and 6(c) illustrate extreme cases, which exhibit some behavior differences worth mentioning.

Fig. 6(b) presents the same comparison as Fig. 6(a), but for case 20×14 (see Fig. 3), which presented the highest value of T_m in the set of simulations performed, with wave parameters $H_s = 1.62$ m and $T_m = 11.70$ s. It can be observed that, analogously to the first case, the time series obtained at the inlet showed a free surface elevation similar to the original, but with RMSD of 0.178 m, being almost twice as large as in the previous case. However, RMSD is a dimensional value, which can be larger for a variable with naturally higher values. In this case, H_s is almost 3 times higher than in case 12×05 (Fig. 6(b)), so an increase in RMSD is not unexpected. Nevertheless, it is possible to use a reference metric to normalize RMSD values, such as the root mean square (RMS) [38], which is widely used in the field of electricity to characterize a variable with sinusoidal behavior.

The normalization parameter commonly used is the arithmetic mean (or simple mean), and the ratio between the RMSD and the mean is the

scatter index (SI) [39], which quantifies the RMSD in a dimensionless manner. However, for waves, the arithmetic mean is almost always a poor choice due to the oscillatory nature of η , which results in the mean being close to zero, regardless of the wave height. For this reason, the definition of SI was used, and instead of the arithmetic mean, the RMS was used for normalization.

The RMS of the free surface elevation (η_{RMS}) for case 12×05 (see Fig. 6(a)) was $\eta_{\text{RMS}} = 0.205$ m, which, with a RMSD of 0.092 m, resulted in a SI of $SI_{12 \times 05} = 0.447$. Meanwhile, in case 20×14 (see Fig. 6(b)), with $\eta_{\text{RMS}} = 0.486$ m and RMSD = 0.178 m, the SI was $SI_{20 \times 14} = 0.367$. This indicates that the difference between original and simulated elevations is rather low between the two cases, given the order of magnitude of the free surface elevations.

Furthermore, Fig. 6(a) shows that, at the wave channel inlet, the elevation spectrum closely follows the TOMAWAC spectrum with a small margin of error, as the largest differences occurred from 1×10^{-1} m²/Hz onwards, while the spectrum peak showed values on the order of 1 m²/Hz. This difference is possibly due to the random phase spectrum inserted into the data (which the TOMAWAC spectrum does not have), and to the noise generated by the method used to calculate the spectrum. Additionally, case 20×14 (see Fig. 6(b)) featured waves generally larger than the ones in case 12×05 , so, they were less susceptible to disturbances in their hydrodynamics.

Finally, the third case in Fig. 6(c) (11×20 from Fig. 3) is somewhat opposite to case 20×14 : the period is intermediate, but the wave height is one of the highest recorded for this location, with wave parameters $H_s = 2.34$ m and $T_m = 6.30$ s. The difference from Fig. 6(b) is clear, in which case 20×14 contained much more spaced oscillations of free surface elevation, indicating that waves were shorter.

The RMSD in this third case is 0.371 m, twice the value of case 20×14 , but in compensation, waves are larger, and, consequently the averaged free surface elevation, $\eta_{\text{RMS}} = 0.678$ m, resulting in a scatter index of $SI = 0.548$, higher than the previous cases. This difference is, possibly, caused by the slender nature of the waves. In the 20×14 scenario, waves presented a much larger period and wavelength; in this case, waves are slender, so it is possible that Fluent had greater difficulty in propagating these waves, which ended up dissipating more than others, thus causing the observed difference.

Furthermore, considering H_s values of the 3 verification cases in Fig. 6, the capability of the computational model to generate irregular waves with different wave heights is evident. Therefore, a qualitative verification based on these results is also inferred, in addition to the quantitative verification already presented.

Available power and energy

The goal of WEC studies is to estimate energy, and using complex wave generation methodologies enhances the reliability and realism of simulation results. Simulating WEC devices helps estimate available power, which is often used to characterize a wave energy project. This work focuses on the wave energy capture stage (primary conversion), developing a methodology to integrate realistic sea state data from a specific location with a WEC device to determine its optimal operating range. To do so, in the supplementary material the numerical method proposed was applied in an OWC WEC.

Conclusions

The goal of this study was to bridge the gap between the large-scale spectral representation of sea states and the short-scale fluid-dynamic modeling of WEC device behavior. By transforming the spectrum into a time series of free surface elevation, a sea state was imposed as a boundary condition in a fluid-dynamic model. Using the WaveMIMO methodology and a statistical characterization of the wave climate in Rio Grande, southern Brazil, a numerical procedure was developed to efficiently estimate the available power for conversion during 2014.

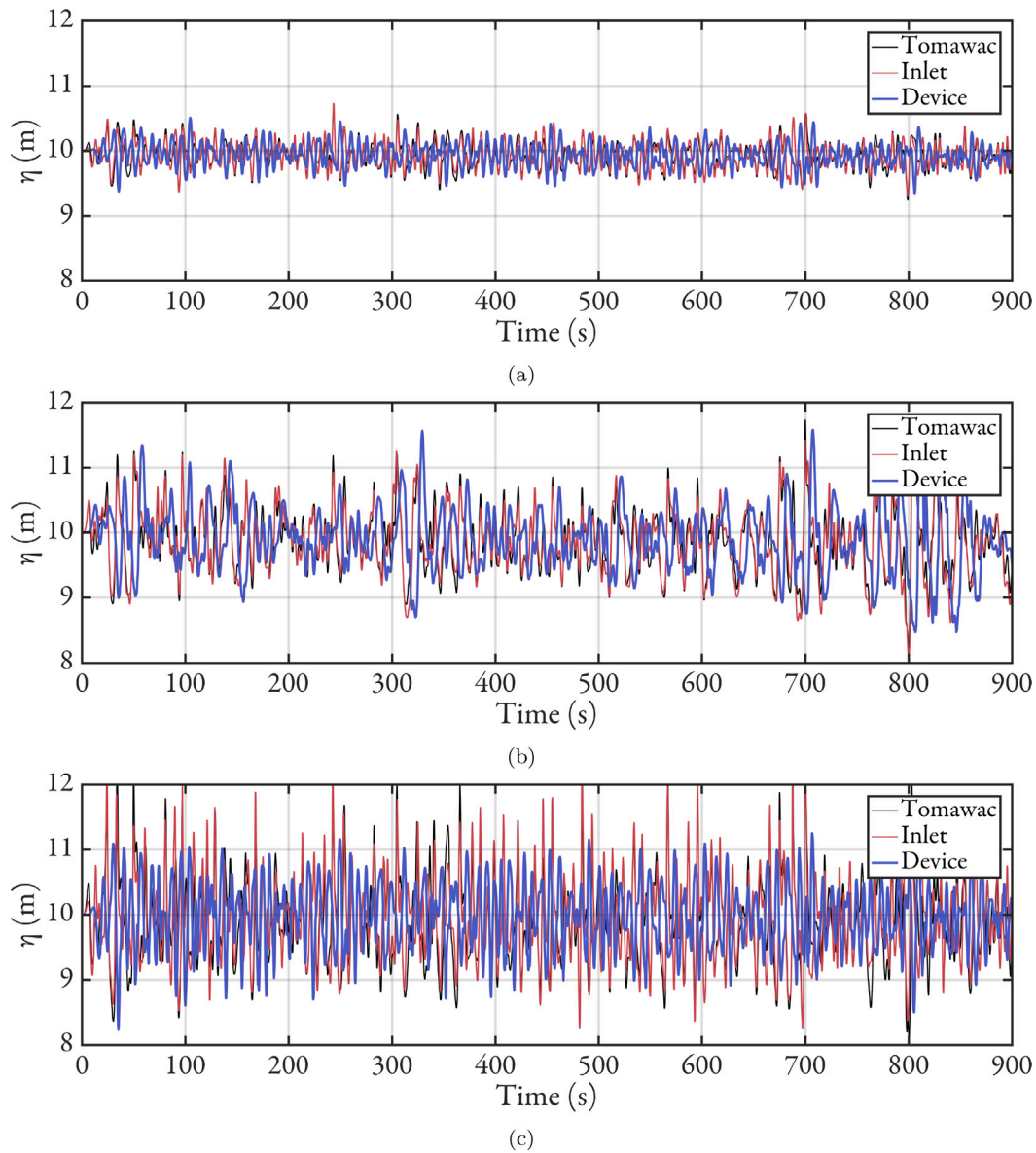


Fig. 6. Comparison of the data from TOMAWAC and Fluent at the wave flume inlet, for cases: (a) 12×05 ($H_s = 0.54$ m and $T_m = 6.90$ s); (b) 20×14 ($H_s = 1.62$ m and $T_m = 11.70$ s); and (c) 11×20 ($H_s = 2.34$ m and $T_m = 6.30$ s).

This numerical method can convert a variance spectrum into a statistically equivalent time series of sea surface elevation, allowing long-term sea state spectra to be represented on short time scales.

Previous studies have shown that regular waves are not adequate predictors of the available power for conversion [36,40], hence the need to use irregular waves. In this context, the results of the present study demonstrated that the proposed methodology adequately represented the imposed sea state in the numerical model, confirming that it can be used for the simulation of irregular waves statistically equivalent to the sea state spectrum used.

To reproduce realistic irregular waves, a calibration of the computational model was carried out aiming to define its spatial and temporal discretizations, defining: inlet segments size (Δz) of 0.4 m, mesh elements size (Δs) of 0.5 m, and time step size (Δt) of 0.05 s (see Tables 1 and 2), with RMSD of 0.1784 m and a processing time reduction around 31% for all 181 performed numerical simulations. After that, the verification of the computational model was performed considering 3 of the 181 cases, which are: $H_s = 0.54$ m and $T_m = 6.90$ s, $H_s = 1.62$ m and $T_m = 11.70$ s, and $H_s = 2.34$ m and $T_m = 6.30$ s; reaching SI values, respectively, of 0.447, 0.367, and 0.548. In

addition, by comparing H_s values of these 3 cases investigated in Fig. 6, one can easily identify the ability of the model to generate irregular waves with different wave heights. Therefore, the computational model was properly verified in quantitative and qualitative ways, proving its capability to represent the different components of a sea state.

Summarizing, in this study, a full year was represented by 181 simulations of 15 min each, representing approximately 0.5% of the original volume of data, thus allowing the estimation of the available energy in a WEC device during a year of operation under realistic sea conditions obtained from a spectral simulation of sea state. Thus, by combining the spectral representation of waves with the time domain representation to generate data for the simulation of WEC devices, it is possible to use this data to estimate the WEC available power. An application of this methodology can be found in the supplementary material of the present work, in which an OWC was investigated. Therefore, this work has achieved its main goal and it is hoped that this will be a step towards adopting renewable energy sources and the supply of global energy demand sustainably.

In future investigations, it is possible to employ the proposed methodology to evaluate different types of WECs, considering other

locations to install them. In addition, the Wave to Wire process is an important approach that will be addressed in future investigations.

CRediT authorship contribution statement

Phelype Haron Oleinik: Writing – review & editing, Writing – original draft, Validation, Software, Methodology, Investigation, Formal analysis, Data curation, Conceptualization. **Rafael Pereira Maciel:** Writing – original draft, Validation, Software, Methodology, Data curation. **Elizaldo Domingues dos Santos:** Writing – review & editing, Visualization, Resources, Project administration, Funding acquisition, Formal analysis. **Luiz Alberto Oliveira Rocha:** Writing – review & editing, Visualization, Resources, Project administration, Funding acquisition, Formal analysis. **Bianca Neves Machado:** Writing – review & editing, Visualization, Supervision, Methodology, Investigation, Formal analysis, Data curation, Conceptualization. **Liércio André Isoldi:** Writing – review & editing, Visualization, Supervision, Resources, Project administration, Methodology, Investigation, Funding acquisition, Formal analysis, Data curation, Conceptualization.

Funding sources

This work was funded by the CAPES, Brazil, Finance Code 001; CNPq, Brazil, Processes: 309648/2021-1, 307791/2019-0, 308396/2021-9, 440010/2019-5, and 440020/2019-0; FAPERGS, Brazil, Process: 21/2551-0002231-0.

Declaration of competing interest

The authors declare the following financial interests/personal relationships which may be considered as potential competing interests: Phelype Haron Oleinik reports financial support was provided by Coordination of Higher Education Personnel Improvement. Rafael Pereira Maciel reports financial support was provided by National Council for Scientific and Technological Development. Elizaldo Domingues dos Santos reports financial support was provided by National Council for Scientific and Technological Development. Luiz Alberto Oliveira Rocha reports financial support was provided by National Council for Scientific and Technological Development. Liércio André Isoldi reports financial support was provided by National Council for Scientific and Technological Development. Liércio André Isoldi reports financial support was provided by Foundation for Research Support of Rio Grande do Sul State. If there are other authors, they declare that they have no known competing financial interests or personal relationships that could have appeared to influence the work reported in this paper.

Acknowledgments

The authors thank the Brazilian funding agencies CAPES (Coordination for the Improvement of Higher Education Personnel), CNPq (National Council for Scientific and Technological Development), and FAPERGS (Research Support Foundation of the State of Rio Grande do Sul). The authors also thank the Federal University of Rio Grande do Sul - UFRGS and Federal University of Rio Grande - FURG for their support in conducting this research.

Supplementary data

Supplementary material related to this article can be found online at <https://doi.org/10.1016/j.seta.2024.104093>.

Data availability

Data will be made available on request.

References

- [1] International Energy Agency. Renewables 2021—Analysis and forecast to 2026. 2021-12-01, URL <https://www.iea.org/reports/renewables-2021>.
- [2] Mørk G, Barstow SF, Kabuth A, Pontes MT. Assessing the global wave energy potential. In: Proceedings of OMAE2010. Shanghai: American Society of Mechanical Engineers; 2010, p. 8.
- [3] Gunn K, Stock-Williams C. Quantifying the global wave power resource. *Renew Energy* 2012;44:296–304. <http://dx.doi.org/10.1016/j.renene.2012.01.101>.
- [4] Reguero BG, Losada IJ, Méndez FJ. A global wave power resource and its seasonal, interannual and long-term variability. *Appl Energy* 2015;148:366–80. <http://dx.doi.org/10.1016/j.apenergy.2015.03.114>.
- [5] Guo B, Ringwood JV. A review of wave energy technology from a research and commercial perspective. *IET Renew Power Gen* 2021;15(14):3065–90. <http://dx.doi.org/10.1049/rpg2.12302>, URL <https://ietresearch.onlinelibrary.wiley.com/doi/10.1049/rpg2.12302>.
- [6] Magagna D, Uihlein A. Ocean energy development in Europe: Current status and future perspectives. *Int J Mar Energy* 2015;11:84–104. <http://dx.doi.org/10.1016/j.ijome.2015.05.001>, URL <http://linkinghub.elsevier.com/retrieve/pii/S2214166915000181>.
- [7] Jin S, Greaves D. Wave energy in the UK: Status review and future perspectives. *Renew Sustain Energy Rev* 2021;143:110932. <http://dx.doi.org/10.1016/j.rser.2021.110932>, URL <https://www.sciencedirect.com/science/article/abs/pii/S1364032121002240>.
- [8] Wimalaratna YP, Hassan A, Afrouzi HN, Mehranzamir K, Ahmed J, Siddique BM, Liew SC. Comprehensive review on the feasibility of developing wave energy as a renewable energy resource in Australia. *Clean Energy Syst* 2022;3:100021. <http://dx.doi.org/10.1016/j.cles.2022.100021>, URL <https://www.sciencedirect.com/science/article/pii/S2772783122000206>.
- [9] Reguero B, Méndez F, Losada I. Variability of multivariate wave climate in latin america and the caribbean. *Glob Planet Change* 2013;100:70–84. <http://dx.doi.org/10.1016/j.gloplacha.2012.09.005>.
- [10] Neill SP, Lewis MJ, Hashemi MR, Slater E, Lawrence J, Spall SA. Inter-annual and inter-seasonal variability of the orkney wave power resource. *Appl Energy* 2014;132:339–48. <http://dx.doi.org/10.1016/j.apenergy.2014.07.023>.
- [11] Mortlock TR, Goodwin ID. Directional wave climate and power variability along the southeast Australian shelf. *Cont Shelf Res* 2015;98:36–53. <http://dx.doi.org/10.1016/j.csr.2015.02.007>.
- [12] Oleinik PH, Marques WC, Kirinus Ed. Estimate of the wave climate on the most energetic locations of the south-southeastern Brazilian shelf. *Defect Diffus Forum* 2017;370:130–40. <http://dx.doi.org/10.4028/www.scientific.net/DDF.370.130>, URL <http://www.scientific.net/DDF.370.130>.
- [13] Oleinik PH, Kirinus Ed, Fragassa C, Marques WC, Costi J. Energetic potential assessment of wind-driven waves on the south-southeastern Brazilian shelf. *J Mar Sci Eng* 2019;7(2):25. <http://dx.doi.org/10.3390/jmse7020025>, URL <https://www.mdpi.com/2077-1312/7/2/25>.
- [14] Machado BN, Oleinik PH, Kirinus Ed, dos Santos ED, Rocha LAO, Gomes MdN, Conde JMP, Isoldi LA. WaveMIMO methodology: Numerical wave generation of a realistic sea state. *J Appl Comput Mech* 2021;7(4):2129–48. <http://dx.doi.org/10.22055/jacm.2021.37617.3051>.
- [15] Oleinik PH, Tavares GP, Machado BN, Isoldi LA. Transformation of water wave spectra into time series of surface elevation. *Earth* 2021;2(4):997–1005. <http://dx.doi.org/10.3390/earth2040059>.
- [16] Benoit M, Marcos F, Becq F. Development of a third generation shallow-water wave model with unstructured spatial meshing. In: 25th international conference on coastal engineering: book of abstracts. New York: American Society of Civil Engineers; 1996, p. 465–78.
- [17] Awk T. Tomawac user manual version 7.2. 2017, The Telemac-Mascaret Consortium. URL www.opentelemac.org.
- [18] Wessel P, Smith WHF. A global self-consistent, hierarchical, high-resolution geography database. *J Geophys Res* 1996;101(B4):8741–3.
- [19] Oleinik PH, Marques WC, Kirinus Ed. Evaluation of the seasonal pattern of wind-driven waves on the south-southeastern Brazilian shelf. *Defect Diffus Forum* 2017;370:141–51. <http://dx.doi.org/10.4028/www.scientific.net/DDF.370.141>, URL <http://www.scientific.net/DDF.370.141>.
- [20] Kirinus Ed, Oleinik PH, Costi J, Marques WC. Long-term simulations for ocean energy off the Brazilian coast. *Energy* 2018;163:364–82. <http://dx.doi.org/10.1016/j.energy.2018.08.080>, URL <https://linkinghub.elsevier.com/retrieve/pii/S0360544218316128>.
- [21] Hasselmann K, Barnett TP, Bouws E, Carlson H, Cartwright DE, Enke K, Ewing JA, Gienapp H, Hasselmann DE, Kruseman P, Meerburg A, Müller PM, Olbers DJ, Richter K, Sell W, Walden H. Measurements of wind-wave growth and swell decay during the Joint North Sea Wave Project (JONSWAP). *Tech. rep., Deutsches Hydrographisches Institut*; 1973, URL <http://resolver.tudelft.nl/uuid:f204e188-13b9-49d8-a6dc-4fb7c20562fc>.
- [22] Cardoso SD, Marques WC, Kirinus Ed, Stringari CE. Levantamento batimétrico usando cartas náuticas. In: 13ª mostra da produção universitária. Rio Grande: Universidade Federal do Rio Grande; 2014, p. 2.

- [23] Freedman D, Diaconis P. On the histogram as a density estimator: L_2 theory. *Z Wahrscheinlichkeitstheor Verwandte Geb* 1981;57(4):453–76. <http://dx.doi.org/10.1007/bf01025868>.
- [24] Versteeg HK, Malalasekera W. *An introduction to computational fluid dynamics*. second ed.. Prentice Hall; 2007.
- [25] ANSYS Inc. ANSYS Fluent Tutorial Guide. Release 18.0. ANSYS Inc.; 2017, URL www.ansys.com/products/fluids/ansys-fluent.
- [26] Park J-C, Kim M-H, Miyata H. Fully non-linear free-surface simulations by a 3D viscous numerical wave tank. *Internat J Numer Methods Fluids* 1999;29(6):685–703. [http://dx.doi.org/10.1002/\(sici\)1097-0363\(19990330\)29:6<685::aid-flid807>3.0.co;2-d](http://dx.doi.org/10.1002/(sici)1097-0363(19990330)29:6<685::aid-flid807>3.0.co;2-d), URL [https://onlinelibrary.wiley.com/doi/10.1002/\(SICI\)1097-0363\(19990330\)29:6%3C685::AID-FLD807%3E3.0.CO;2-D#](https://onlinelibrary.wiley.com/doi/10.1002/(SICI)1097-0363(19990330)29:6%3C685::AID-FLD807%3E3.0.CO;2-D#).
- [27] Lisboa RdC, Teixeira PRd, Didier E. Regular and irregular wave propagation analysis in a flume with numerical beach using a Navier-Stokes based model. *Defect Diffus Forum* 2017;372:81–90. <http://dx.doi.org/10.4028/www.scientific.net/DDF.372.81>.
- [28] Gomes MN, Lorenzini G, Rocha LA, dos Santos ED, Isoldi LA. Constructal design applied to the geometric evaluation of an oscillating water column wave energy converter considering different real scale wave periods. *J Eng Thermophys* 2018;27(2):173–90. <http://dx.doi.org/10.1134/S1810232818020042>.
- [29] Noh WF, Woodward P. SLIC (simple line interface calculation). In: *Proceedings of the fifth international conference on numerical methods in fluid dynamics June 28 – July 2, 1976 twente university, enschede*. Springer Berlin Heidelberg; 1976, p. 330–40.
- [30] Hirt CW, Nichols BD. Volume of fluid (VOF) method for the dynamics of free boundaries. *J Comput Phys* 1981;39(1):201–25. [http://dx.doi.org/10.1016/0021-9991\(81\)90145-5](http://dx.doi.org/10.1016/0021-9991(81)90145-5), URL <https://www.sciencedirect.com/science/article/pii/0021999181901455>.
- [31] Rienecker MM, Fenton JD. A Fourier approximation method for steady water waves. *J Fluid Mech* 1981;104:119. <http://dx.doi.org/10.1017/S0022112081002851>, URL <http://www.journals.cambridge.org/abstract/S0022112081002851>.
- [32] Chang H-K, Lin S-C. An explicit approximation to the wavelength of nonlinear waves. *Ocean Eng* 1999;26:147–60.
- [33] Dean RG, Dalrymple RA. *Water wave mechanics for engineers and scientists. Advanced series on ocean engineering. Vol. 2*, World Scientific Publishing Company; 1991, p. 368.
- [34] Chakrabarti S. *Handbook of offshore engineering*. Elsevier; 2005.
- [35] Martins JC, Goulart MM, Gomes MdN, Souza JA, Rocha LAO, Isoldi LA, dos Santos ED. Geometric evaluation of the main operational principle of an overtopping wave energy converter by means of constructal design. *Renew Energy* 2018;118:727–41. <http://dx.doi.org/10.1016/j.renene.2017.11.061>.
- [36] Hübner RG, Fragassa C, da S. Paiva M, Oleinik PH, das N. Gomes M, Rocha LAO, dos Santos ED, Machado BN, Isoldi LA. Numerical analysis of an overtopping wave energy converter subjected to the incidence of irregular and regular waves from realistic sea states. *J Mar Sci Eng* 2022;10:20. <http://dx.doi.org/10.3390/jmse10081084>.
- [37] Neill SP, Hashemi MR. Chapter 8 - ocean modelling for resource characterization. In: Neill SP, Hashemi MR, editors. *Fundamentals of ocean renewable energy. E-business solutions*, Academic Press; 2018, p. 193–235. <http://dx.doi.org/10.1016/B978-0-12-810448-4.00008-2>.
- [38] Holthuijsen LH. *Waves in oceanic and coastal waters*. first ed.. Cambridge: Cambridge University Press; 2007, p. 387.
- [39] Chawla A, Spindler DM, Tolman HL. Validation of a thirty year wave hindcast using the Climate Forecast System Reanalysis winds. *Ocean Model* 2013;70:189–206.
- [40] Teixeira PR, Didier E. Numerical analysis of the response of an onshore oscillating water column wave energy converter to random waves. *Energy* 2021;220:119719. <http://dx.doi.org/10.1016/j.energy.2020.119719>.